Supporting Information

Large Enhancement of Thermoelectric Properties in n-type PbTe via dual-site point defects

Liangwei Fu,[‡ab] Meijie Yin,[‡ab] Di Wu,[a] Wei Li,[a] Dan Feng,[a] Li Huang*[a] and Jiaqing He*[a]

[a] Shenzhen Key Laboratory for Thermoelectric Materials and Department of Physics, Southern University of Science and Technology, Shenzhen, 518055, China

[b] School of Physics and Technology, Wuhan University, Wuhan 430072, China

‡These authors contributed equally to this work.

* To whom correspondence should be addressed.

E-mail: he.jq@sustc.edu.cn; huangl@sustc.edu.cn

This supporting information includes: Figure S1~S9, Table S1-S2 and the density function theory (DFT) and lattice thermal conductivity calculation.

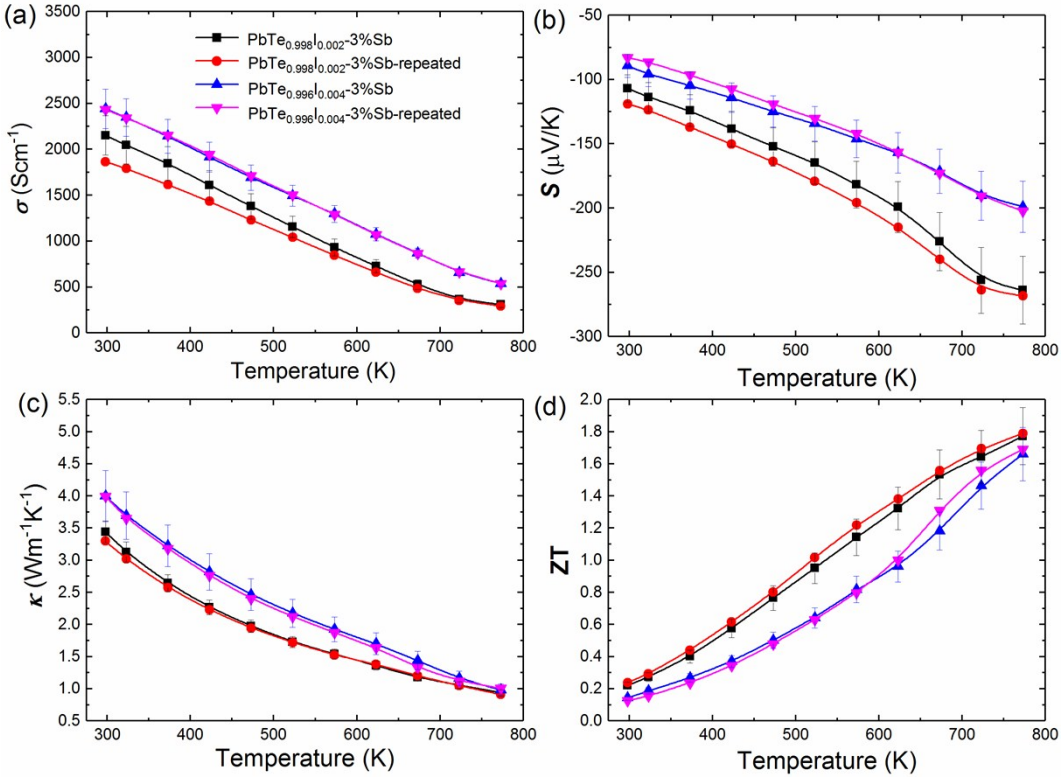

Figure S1 The repeatability test of $PbTe_{0.998}I_{0.002}$-3%Sb and $PbTe_{0.996}I_{0.004}$-3%Sb samples. (a)-(d) The temperature dependence of the electrical transport properties, (a) the electrical conductivity, (b) the Seebeck coefficient, (c) the total thermal conductivity, (d) the ZT values.

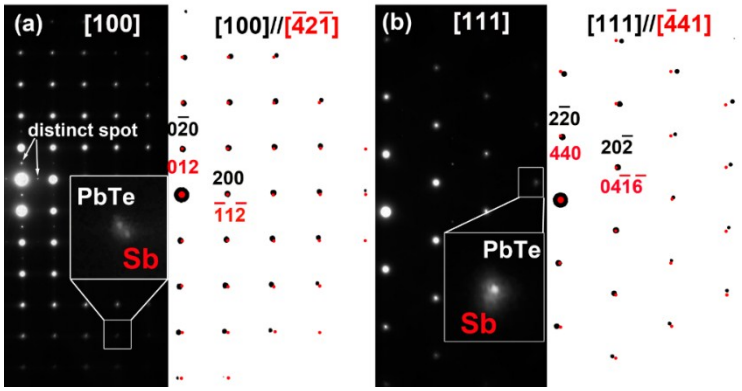

Figure S2. (a) and (b) the left hand sides of these two figures show the experimental selected area electron diffraction patterns along the [100] and [111] zone axes of PbTe matrix respectively, and the right and side of these two figures show the calculated overlaping electron diffraction patterns of PbTe and Sb, where the black one corresponds to the electron diffraction pattern along the [100] and [111] zone axes of PbTe and the red one corresponds to that along the [4̄2T] and [4̄41] zone axes of Sb. The insets show the magnification images of selected diffraction dots.

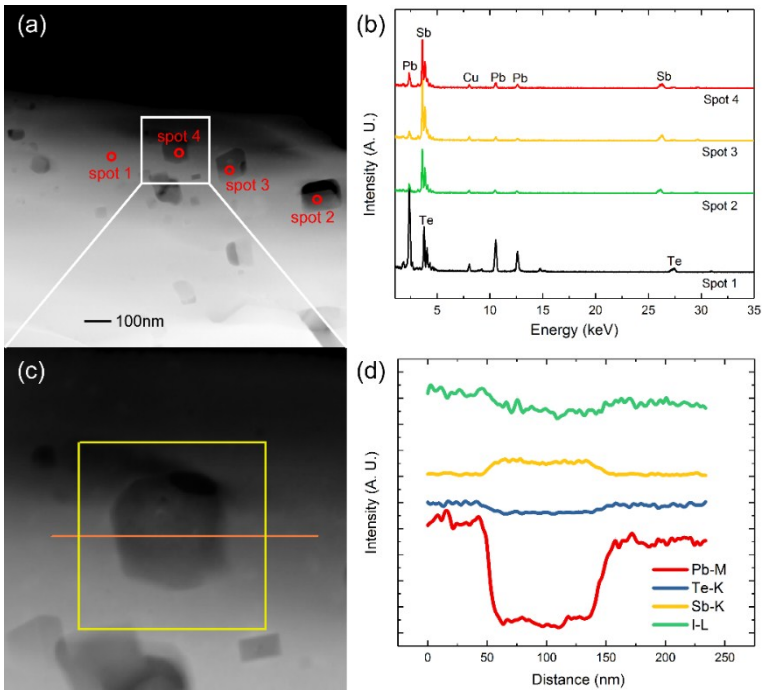

Figure S3 The EDS point analysis and line analysis on the $PbTe_{0.998}I_{0.002}$-3%Sb sample. (a) the low magnified STEM image of $PbTe_{0.998}I_{0.002}$-3%Sb sample. Four points were selected, which are indicated by red circles. (b) the EDS spectrum of the selected four points. (c) the line analysis (along the orange line) on a typical nano-precipitate. (d) the EDS spectrum of Pb-M, Te-K, Sb-K, I-L, respectively, corresponding to the line analysis. Due to the energy peaks of Te-L and Sb-L is very close to each other and hard to distiguish, the Te-K and Sb-K peak are used instead.

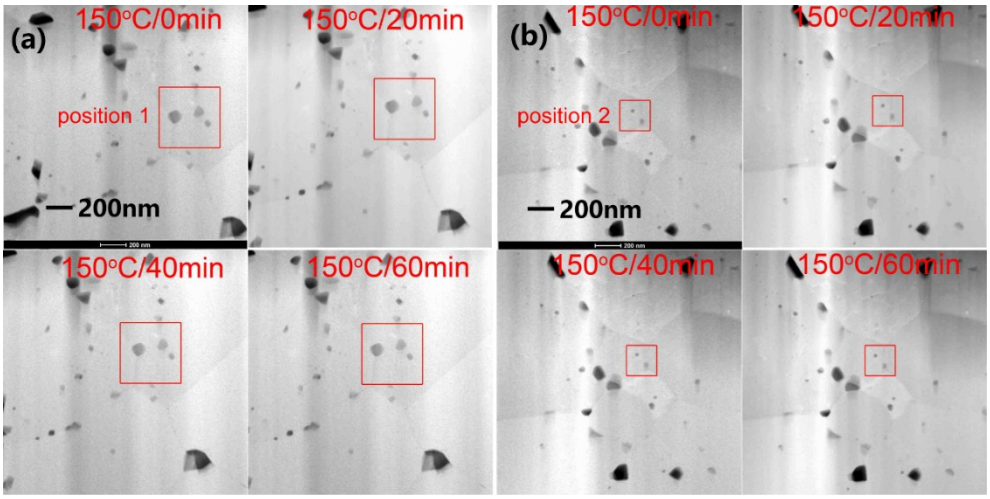

Figure S4 The *in situ* TEM experiment at 150℃ on the $PbTe_{0.998}I_{0.002}$-3%Sb composite sample. The thin film sample was under radiation of electron beam for about 60 minutes. Two randomly selected positions are indicated by red squares: (a) position 1, (b) position 2. The nano scale dark-contrast areas are the Sb nano-precipitates. The screen current and does rate used during the radiation were 0.04 nA and 8 $enm^{-2}s^{-1}$, respectively.

The density function theory (DFT) calculation

The first-principles DFT calculations are performed using the projector-augmented wave (PAW) method, as implemented in Vienna *Ab initio* Simulation Package.[1-5] The exchange-correlation interaction is treated in the generalized gradient approximation (GGA) of Perdew, Burke, Ernzerholf (PBE). The Kohn-Sham orbitals are expanded in plane waves with an energy cutoff of 550eV. The energy convergence criterion is chosen to be 10^{-4}eV and the Hellman-Feynman forces on all atoms are below 0.01eV/Å. Spin-orbit coupling (SOC) effects are also included because the heavy elements present in this material. The optimized lattice parameters are found to be a = b = c = 6.569 Å, which is in good agreement with the experimental values.[6] A 2×2×2 supercell is used to model the cubic PbTe. A Monkhorst-Pack Γ-centered 5×5×5 k-point grid is used for Brillouin zone sampling.

The formation energy E_f of a defect D in the charge state of q is given by

$$E_f(D,q) = E_{tot}(D, q) - E_{tot}(0) - \sum n_i\mu_i + q(E_{VBM} + E_F + \Delta V) \qquad (S1)$$

Where $E_{tot}(D, q)$ and $E_{tot}(0)$ are the total energies of the supercell with and without the defect. E_F is the Fermi level with respect to the valence band maximum (VBM) of the host system, E_{VBM}, in the defect-free supercell.[7] For non-degenerate semiconductors valid values of E_F range from the VBM to the conduction band minimum (CBM), i.e., from 0 to the value of the band gap. The defect is created by adding (positive) or removing (negative) n_i atoms with chemical potential μ_i, which depends on the experimental condition under which the material

is grown, from the defect-free supercell. In this calculation, μ_{Pb} and μ_{Te} are obtained from the most stable pure phases, the elemental bulk systems. While μ_{Sb} is obtained from the Sb_2Te_3 in order to avoid the formation of the second phases. In a periodic supercell, an absolute reference potential is ill-defined, and the calculated eigenvalue spectra from different calculations are not directly comparable. So an alignment term ΔV is added to align the electrostatic potentials between the defect and the pure cells, a common reference (the deep *1s* core levels of the atoms far away from the defects) is used in our approach.[8]

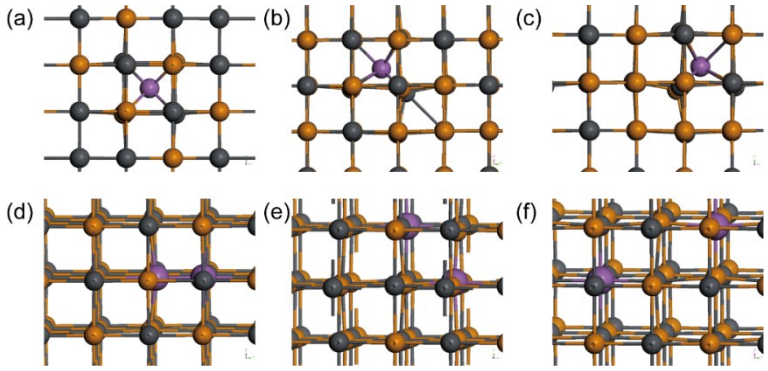

Figure S5 The relaxed crystal structures of the supercells having Sb_i (a), Sb_{Pb}+Pb_i (b), Sb_{Te}+Te_i(c), Sb_{Pb}+Sb_{Te} nearest neighbor (d), Sb_{Pb}+Sb_{Te} next nearest neighbor (e), Sb_{Pb}+Sb_{Te} third nearest neighbor (f) defects, respectively.

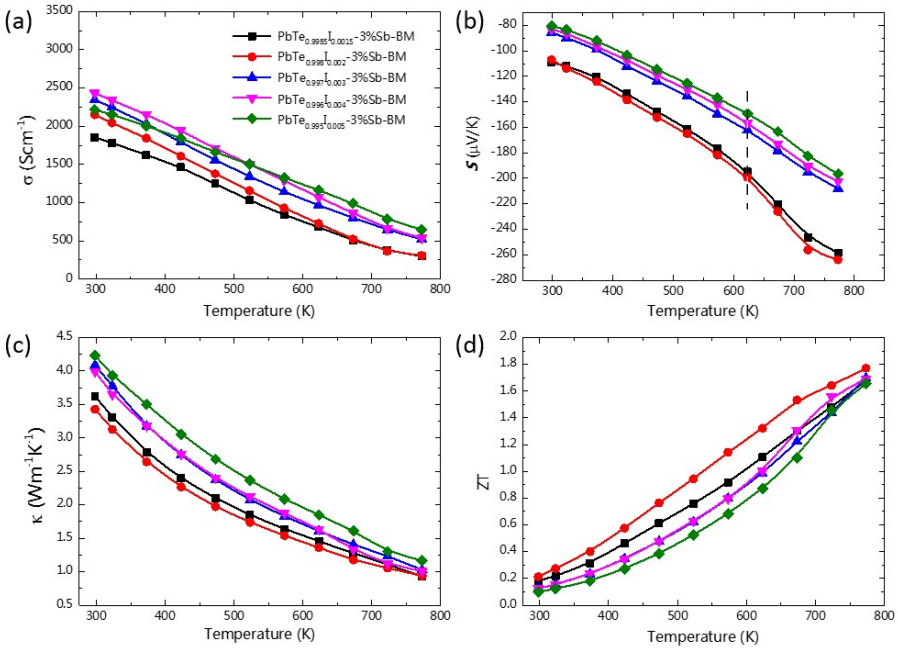

Figure S6 (a)-(d) the temperature dependence of the electrical transport properties of the $PbTe_{1-y}I_y$-3%Sb (y=0.0015~0.005) samples, (a) the electrical conductivity, (b) the Seebeck coefficient, (c) the total thermal conductivity, (d) the ZT values. The temperature corresponding to the sudden increase of Seebeck coefficient is indicated by a black doted line.

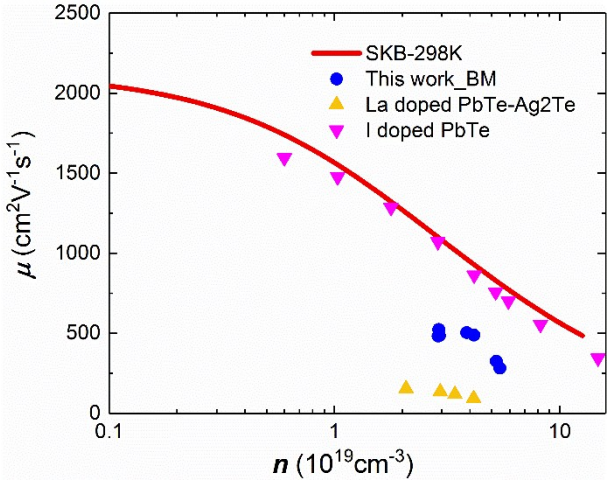

Figure S7 The carrier concentration dependence of carrier mobility of studies samples at 298K. The red lines are calculated based on the single Kane band model and only the acoustic phonon scattering is considered. The purple and yellow triangles correspond to the mobility values of I doped PbTe materials [9] and PbTe/Ag_2Te composites [10].

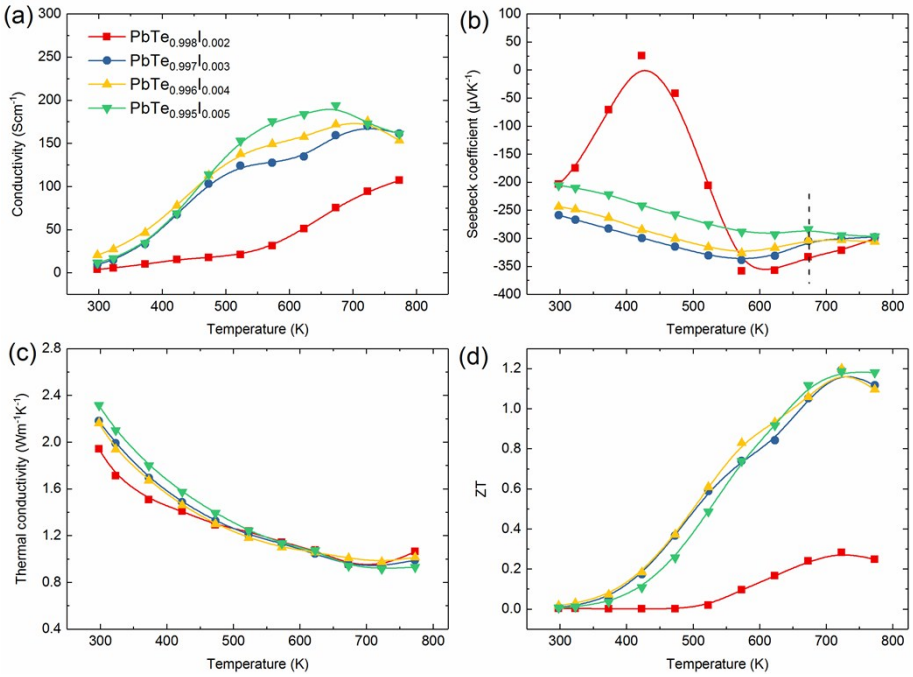

Figure S8 (a)-(d) the temperature dependence of the electrical transport properties of the $PbTe_{1-y}I_y$ (y=0.002~0.005) samples, (a) the electrical conductivity, (b) the Seebeck coefficient, (c) the total thermal conductivity, (d) the ZT values. The temperature corresponding to the sudden increase of Seebeck coefficient is indicated by a black doted line.

Table S1 Relative density and electrical transport parameters of the $PbTe_{1-y}I_y$ (y=0.002~0.005) samples at room temperature

Sample ID	n $10^{19}cm^{-3}$	μ $cm^2V^{-1}s^{-1}$	Relative density
$PbTe_{0.998}I_{0.002}$	0.051	20.6	96%
$PbTe_{0.997}I_{0.003}$	0.314	20.9	96.6%
$PbTe_{0.996}I_{0.004}$	0.396	29.9	99.0%
$PbTe_{0.995}I_{0.005}$	0.711	5.23	98.0%
$PbTe_{0.9985}I_{0.0015}$-3%Sb	2.91	524	97.9%
$PbTe_{0.998}I_{0.002}$-3%Sb	2.93	458	98.2%
$PbTe_{0.997}I_{0.003}$-3%Sb	4.16	489	98.9%
$PbTe_{0.996}I_{0.004}$-3%Sb	5.24	333	98.4%
$PbTe_{0.995}I_{0.005}$-3%Sb	5.43	282	97.6%

Calculation of lattice thermal conductivity

To understand the mechanisms of phonon scattering in this PbTe-based system, theoretical calculation based on the modified Callaway's model is conducted. According to the Callaway's model,[11] the lattice thermal conductivity is expressed as:

$$\kappa_L = \frac{k_B}{2\pi^2 v_a}\left(\frac{k_B T}{\hbar}\right)^3 \int_0^{\theta_D/T} \tau_c \frac{e^x}{(e^x-1)^2} x^4 dx \quad (1)$$

where x is defined as $\hbar\omega/k_BT$, k_B is the Boltzmann's constant, $\hbar$ is reduced Plank constant, v_a is an averaged phonon group velocity, T is absolute temperature and is Debye temperature. The τ_c is a combined term, which relates to many phonon scattering mechanisms. In this paper, only the scattering from Umklapp process (τ_U), Normal process (τ_N), point defects (τ_{PD}), and precipitates (τ_P) were considered, thus,

$$\tau_c^{-1} = \tau_U^{-1} + \tau_N^{-1} + \tau_{PD}^{-1} + \tau_P^{-1} \quad (2)$$

The first two contributions originate mainly from the matrix. The point defect scattering of iodine is not considered in the calculation for its tiny content.

It should be pointed out that among all the parameters used to calculted the temperature dependent κ_L of the $PbTe_{0.996}I_{0.004}$ (U+N) and $PbTe_{0.998}I_{0.002}$-3%Sb (U+N+P) based on the Callaway's model, there is one fitting parameter, ratio of normal phonon scattering to Umklapp scattering, β. We obtained the ratio of normal phonon scattering to Umklapp scattering, β, by fit the lattice thermal conductivity of $PbTe_{0.996}I_{0.004}$ sample using the U+N processes based on Callaway's model, shown in **Figure S9**. The value of β in this work is 2.9, which is close to the reported one, 2.5, used for PbTe materials[12]. The phonon-scattering effect of iodine doping is neglected duo its low content. The deviation from experimental values in the high temperature range (>673K) is doe to bipolar effect caused by thermal activation.

We figured out the temperature dependent amount of dissolved Sb (x_{Sb}). As the total amount of Sb is 3%, the the amount of Sb existing as nano-precipitates (x_P) is equal to 3%-x_{Sb}. For

convenience, we assumed that the number density of nanoscale precipitates (Vp) is propotion to the amount of Sb nano-precipitates (x_P) in all the temperature range. By using the results of temperature dependten x_{Sb} *and* V_P, we calculated the theoretical κ_L in temperature range of 323K~673K.

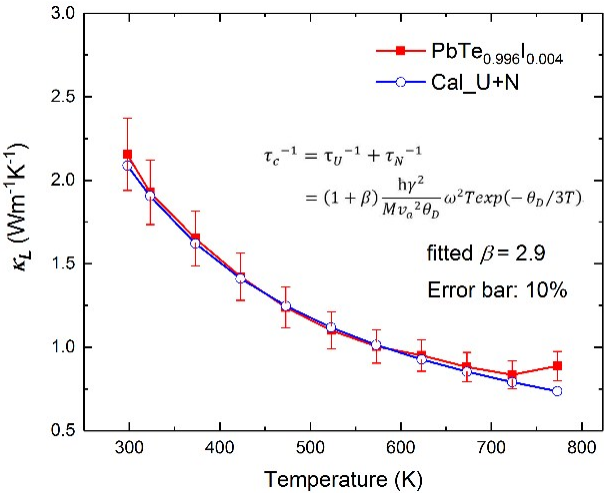

Figure S9 The experimental and calculated lattice thermal conductivity of $PbTe_{0.996}I_{0.004}$ sample.

Table S2 Input parameters for calculation of relaxation time of phonon scattering for $PbTe_{0.998}I_{0.002}$-3%Sb composite (U+N+P) and assumed $Pb_{0.9852}Sb_{0.0148}Te_{0.9852}Sb_{0.0148}$ alloy (U+N+PD).

Relaxation time	Parameters	Symbol	Value	
			$PbTe_{0.998}I_{0.002}$-3%Sb	$Pb_{0.9852}Sb_{0.0148}Te_{0.9852}Sb_{0.0148}$
$\tau_U^{-1} = \frac{\hbar\gamma^2}{M v_a^2 \theta_D}\omega^2 T exp(-\theta_D/3T)$; $v_a = \left[\frac{1}{3}\left(\frac{1}{v_L^3} + \frac{2}{v_T^3}\right)\right]^{-\frac{1}{3}}$; $v_p = \frac{1-2(v_T/v_L)^2}{2-2(v_T/v_L)^2}$;	Gruneisen parameter	γ	1.96 [13]	1.96 [13]
	Longitudinal sound velocity	v_L (m/s)	2919	2919
	Transversal sound velocity	v_T (m/s)	1620	1620
	Average sound velocity	v_a (m/s)	1805	1805
	Debye temperature	θ_D(K)	136 [13]	136 [13]
	Average mass of an atom	M (kg)	2.78	2.77
	Poisson ratio	v_p	0.28	0.28
$\tau_N^{-1} = \beta\tau_U^{-1}$;	**Ratio of normal phonon scattering to Umklapp scattering**	$\boldsymbol{\beta}$	**2.9 (fitting)**	**2.9 (fitting)**
$\tau_{PD}^{-1} = \frac{\omega^4 V_0}{4\pi v_a^3}(\Gamma_M + \Gamma_S)$; $\Gamma_M = \frac{1}{2}\sum_{i=1}^{n}\left(\frac{\bar{M}_i}{\bar{\bar{M}}}\right)^2 f_i^1 f_i^2 \left(\frac{M_i^1 - M_i^1}{\bar{M}_i}\right)^2$; $\Gamma_S = \frac{1}{2}\sum_{i=1}^{n}\left(\frac{\bar{M}_i}{\bar{\bar{M}}}\right)^2 f_i^1 f_i^2 \varepsilon\left(\frac{r_i^1 - r_i^1}{\bar{r}_i}\right)^2$; $\bar{M}_i = \sum_k f_i^k M_i^k$; $\bar{\bar{M}} = \frac{1}{2}\sum_{i=1}^{n}\bar{M}_i$; $\varepsilon = \frac{2}{9}\left[\frac{6.4\gamma(1+v_p)}{1-v_p}\right]^2$;[14]	Phenomenological parameter	ε	--	110
	Mole mass of Pb, Te, Sb	M_{Pb} (g/mol) M_{Te} (g/mol) M_{Sb} (g/mol)	-- -- --	207.2 127.6 121.76
	Radius of Pb, Te, Sb atoms	r_{Pb} (pm) r_{Te} (pm) r_{Sb} (pm)	-- -- --	175 143 136
	Fractional occupant	f_{Pb} f_{Te} f_{Sb}	1 1 0	f_{Pb}: 0.9852 f_{Te}: 0.9852 f_{Sb} at Pb site: 0.0148, f_{Sb} at Te site: 0.0148
	The number of sublattices	n	--	2
	The ordinal value of atom species at each sublattice	k	Pb: 1; Te: 1;	Pb: 1, 2; Te: 1, 2;
	Volume per atom	V_0 (Å^3)	--	33.69
	The ordinal value of sublattice	i	1, 2;	1, 2;
$\tau_P^{-1} = v_a(\sigma_s^{-1} + \sigma_l^{-1})^{-1} V_P$ $\sigma_s = 2\pi R^2$ $\sigma_l = \frac{4}{9}\pi R^2\left(\frac{\Delta D}{D_{PbTe}}\right)^2\left(\frac{\omega R}{v_a}\right)^4$ $\Delta D = D_{PbTe} - D_{Sb}$	Average radius of nanoscale precipitates	R (nm)	23.5	--
	Mass density of PbTe	D_{PbTe} (gcm^{-3})	8.24	--
	Mass density of Sb	D_{Sb} (gcm^{-3})	6.7	--
	Number density of nanoscale precipitates	V_P (m^{-3})	1.910×10^{20}	--

References

1. G. Kresse and J. Furthmüller, *Physical Review B*, 1996, **54**, 11169.
2. G. Kresse and J. Furthmüller, *Computational Materials Science*, 1996, **6**, 15-50.
3. J. P. Perdew and Y. Wang, *Physical Review B*, 1992, **45**, 13244.
4. P. E. Blöchl, *Physical Review B*, 1994, **50**, 17953.
5. G. Kresse and D. Joubert, *Physical Review B*, 1999, **59**, 1758.
6. G. Tan, F. Shi, S. Hao, L.-D. Zhao, H. Chi, X. Zhang, C. Uher, C. Wolverton, V. P. Dravid and M. G. Kanatzidis, *Nat Commun*, 2016, **7**, 12167.
7. C. G. Van de Walle and J. Neugebauer, *Journal of Applied Physics*, 2004, **95**, 3851-3879.
8. S. Chen, A. Walsh, X. G. Gong and S. H. Wei, *Advanced materials*, 2013, **25**, 1522-1539.
9. A. D. LaLonde, Y. Pei and G. J. Snyder, *Energy & Environmental Science*, 2011, **4**, 2090.
10. Y. Pei, J. Lensch-Falk, E. S. Toberer, D. L. Medlin and G. J. Snyder, *Advanced Functional Materials*, 2011, **21**, 241-249.
11. J. He, J. Androulakis, M. G. Kanatzidis and V. P. Dravid, *Nano Letters*, 2012, **12**, 343-347.
12. S.-H. Lo, J. He, K. Biswas, M. G. Kanatzidis and V. P. Dravid, *Advanced Functional Materials*, 2012, **22**, 5175-5184.
13. J. He, S. N. Girard, M. G. Kanatzidis and V. P. Dravid, *Advanced Functional Materials*, 2010, **20**, 764-772.
14. C. L. Wan, W. Pan, Q. Xu, Y. X. Qin, J. D. Wang, Z. X. Qu and M. H. Fang, *Physical Review B*, 2006, **74**.